Role of gp120 Trimerization on HIV Binding Elucidated with Brownian Adhesive Dynamics

Andrew D. Trister and Daniel A. Hammer
Department of Bioengineering, University of Pennsylvania, Philadelphia, Pennsylvania

ABSTRACT We simulated the docking of human immunodeficiency virus (HIV) with a cell membrane using Brownian adhesive dynamics. The main advance in the current version of Brownian adhesive dynamics is that we use a simple bead-spring model to coarsely approximate the role of gp120 trimerization on HIV docking. We used our simulations to elucidate the effect of *env* spike density on the rate and probability of HIV binding, as well as the probability that each individual gp120 trimer is fully engaged. We found that for typical CD4 surface densities, viruses expressing as few as 8 *env* spikes will dock with binding rate constants comparable to viruses expressing 72 spikes. We investigated the role of cellular receptor diffusion on the degree of binding achieved by the virus on both short timescales (where binding has reached steady state but before substantial receptor accumulation in the viral-cell contact zone has occurred) and long timescales (where the system has reached steady state). On short timescales, viruses with 10–23 *env* trimers most efficiently form fully engaged trimers. On long timescales, all gp120 in the contact area will become bound to CD4. We found that it takes seconds for engaged trimers to cluster CD4 molecules in the contact zone, which partially explains the deleay in viral entry.

INTRODUCTION

Human immunodeficiency virus (HIV) is the cause of acquired immunodeficiency syndrome (AIDS), and currently afflicts 33,000,000 people worldwide and was responsible for 2,000,000 deaths in 2006 (1). While the progress of HIV infection to AIDS has been effectively slowed with pharmaceuticals in many patient populations, HIV infection continues to be a worldwide public health concern (2). A greater understanding of the molecular mechanisms of viral pathogenesis can explain viral tropism as well as the variation in virulence seen in different hosts. A robust description of the molecular basis of disease may lead to better targeted therapies against infection and improved methods to monitor disease progression.

The first step in viral infection is the binding of receptor and ligand allowing the viral particle to dock to a host cell (3). HIV expresses protein spikes on the viral envelope that are derived from the *env* sequence of the viral genome. The envelope spike has two noncovalently bound subunits, gp41 and gp120. Each spike on the viral envelope consists of a trimer of gp120 and gp41 (4). Viral docking is initiated by gp120 binding its primary target, CD4, expressed on the surface of host cells. Upon binding to CD4, the gp120-CD4 complex begins to dissociate from gp41 and a cryptic coreceptor binding site is revealed on gp120. The complex must bind a coreceptor to further dissociate gp120 from gp41, freeing gp41 to interact with the host cell membrane. A conformational shift in gp41 leads to fusion of the viral envelope with the cell membrane. In certain viral strains, each gp120 monomer on an *env* spike must be bound to CD4 and chemokine receptor before fusion of the viral envelope with the cell membrane can occur (5,6).

Once gp41 is free of gp120, it undergoes a coiled-coil interaction similar to hemagglutinin (HA) used by influenza virus and other fusion proteins seen in different enveloped viruses. Previous studies of influenza virus have shown that between six and eight HA binding proteins are needed to bind to a cell surface before the virus can fuse with the cell (7). HIV may require fewer bound gp120 molecules to fuse (5), and studies of the stoichiometry of the fusion complex indicate that a single wild-type homotrimer is sufficient to form a fusion pore (8). In our computer simulations, we investigate the relationship of the spatial configuration of the *env* spike on the probability of the virus having at least a single fully engaged trimer as a function of time, which can be viewed as a metric of the minimum requirement for viral entry.

Different groups have debated the number of *env* proteins on the envelope of a competent HIV virion since the first direct observation of 72 spikes was made by electron microscopy in 1991 (9). Through biochemical analysis and cryo-electron microscopy, other groups have more recently estimated that 2–14 trimers are expressed on a mature virion (10–13). The *env* spike density on the viral envelope can influence both the rate constant of viral binding and the frequency with which the virus will have a fully engaged trimer. We investigate how these two parameters (the rate constant for viral binding and the probability of fully engaged trimers) are affected by *env* density, and determine optimal viral configurations for binding and infection.

We have developed a model of viral docking based on a method previously developed in the Hammer laboratory that combines adhesive dynamics with Brownian motion (BRAD) (14). Adhesive dynamics is a stochastic algorithm to determine

Submitted July 27, 2007, and accepted for publication January 23, 2008.

Address reprint requests to Daniel A. Hammer, Tel.: 215-573-6761; E-mail: hammer@seas.upenn.edu.

Editor: Jason M. Haugh.

0006-3495/08/07/40/14 $2.00

doi: 10.1529/biophysj.107.118430

the adhesion of a biological object by receptor-mediated bond formation; the formation and state of intermolecular bonds are based on the Bell model of bond formation and dissociation (15). Adhesive dynamics has been used extensively to model effects related to leukocyte rolling and adhesion (16–19). Once a bond is formed, the subsequent effects on particle motion are calculated from a force balance of the adhesive and hydrodynamic forces. Each bond is modeled as a Hookean spring and the bonded forces on the particle are calculated from the displacement of these springs. The stochasticity of bond formation and breakage is modeled from a Monte Carlo sampling of a distance-dependent distribution function (20).

BRAD extended the simulation methods of adhesive dynamics to account for the small nanometric objects, such as viruses, where Brownian motion would be significant (21). We previously published two articles employing BRAD for the simulation of viruses binding to cell surfaces, but the limitation was that our methods were ''generic''—we modeled viral attachment proteins as monomers. However, gp120 is known to exist as a trimer, and a simplified bead-spring model has been incorporated into BRAD to account for gp120 trimerization. We use the bead-spring units to coarse-grain the entire *env* spike with three gp120 monomers connected to a gp41 stalk. This coarse-grained model produces a close approximation to the structure of *env* spikes as reproduced by cryo-electron tomography (22). The algorithm is now able to calculate the number of fully engaged trimers, a possible determinant of entry (as suggested above). With this new model, we are able to make predictions regarding the effects of cell surface receptor diffusion on viral docking. We calculate the binding rate constant of viruses with different gp120 densities and we make predictions of the optimum number of spikes for the virus to form fully engaged trimers. The methods described in this article have produced the most complete and general model of the dynamics of HIV docking to the cell membrane available.

MODELS

Brownian motion—adhesive dynamics

Our algorithm is based on previous work on Brownian adhesive dynamics (14). The virus is translated and rotated relative to the planar cell surface. To model the motion of the virion, we balance three forces acting on the viral particle—Brownian forces, bonding forces emerging from gp120-CD4 interactions, and nonspecific cell-virus interaction forces. Brownian forces are caused by the random collision of the surrounding solvent with the viral particle. Bonding forces occur after a bond between the virus and cell surface is formed and then stretched or compressed due to the motion of the virus relative to the cell surface. Nonspecific forces include electrostatic, steric, and van der Waals forces. These forces are all included in solving the Langevin equation of thermally driven random motion. We employ the efficient method of solving the Langevin equation developed by Ermak and McCammon to propagate the motion of the virus (23). The minute displacement of the virus at each time step is modeled as a Markov process with the identity listed in Eq. 1,

$$X^{n+1} = X^n + \left(\frac{\Delta t}{k_B T}\right)\mathbf{D}^n F(X^n) + R^n, \tag{1}$$

$$\langle R(t)\rangle = 0, \tag{2}$$

$$\langle R(t)R(t')^T\rangle = 2\gamma k_B T\,\mathbf{M}\delta(t-t'), \tag{3}$$

where X^n is the position of the virus at time n, Δt is the time step used in the algorithm, k_B is the Boltzmann constant, T is the temperature Kelvin of the system, $\mathbf{D}^n$ is the diffusion tensor at time n, $F(X^n)$ is the sum of extrinsic forces on the virus at position X^n, γ is the friction coefficient, and R^n is the random displacement due to thermal force with distributions shown in Eqs. 2 and 3. $\delta(t–t')$ in Eq. 3 represents the Krönecker delta function.

The virus also undergoes random torques (24) and we describe an analogous set of equations for the rotation of the virus due to random interactions with the surrounding fluid and from the force of the bonds on the virus. The propagation of the effect of random torque on the virus is described in Eq. 4 with random torque distributions in Eqs. 5 and 6,

$$\Theta^{n+1} = \Theta^n + \left(\frac{\Delta t}{k_B T}\right)\mathbf{D}_\omega^n T(\Theta^n) + R_\omega^n, \tag{4}$$

$$\langle R_\omega(t)\rangle = 0, \tag{5}$$

$$\langle R_\omega(t)R_\omega(t')^T\rangle = 2\gamma_\omega k_B T\,\mathbf{I}\delta(t-t'), \tag{6}$$

where Θ^n is the rotational position at time n, $\mathbf{D}_\omega^n$ is the rotational diffusion tensor at time n, $T(\Theta^n)$ is the sum of the extrinsic torques at rotational position Θ^n, γ_ω is the rotational friction coefficient, $\mathbf{I}$ is the moment of inertia for the virus, R_ω^n is the random angular rotation due to thermal torque, and the other constants are as above. We model the virus as a solid sphere in calculating the moment of inertia.

The nonspecific electrosteric forces between the viral envelope and the cell membrane are included in the calculation as a phenomenological equation as shown in based on work by Bell (25) and reproduced in Eq. 7. Phenomenological forms such as these have been used previously in adhesive dynamics simulations to describe the nonspecific interactions between membranes in close apposition (26),

$$F_{rep} = F_0\frac{re^{-rs}}{1-e^{-rs}}, \tag{7}$$

where F_{rep} represents the repulsive force at separation s, F_0 includes the force from the compressibility of the interaction layer, and r is the thickness of the polymer layer between the membranes. We tuned these parameters to values that ensure the membranes can interact at the distance of a gp120-CD4 bond, but produce a repulsive force great enough to ensure the virus does not pass through the cell membrane with values for F_0 of 10^{-18} N and r of 10^{-9} m.

Bond formation and breakage are treated as stochastic processes and we use a modified Monte Carlo scheme to determine the state of individual bonds. At each time step we sample from a probability distribution model for the rates of bond formation and breakage (20). The forward rate is given by Eq. 8, while the reverse rate is shown in Eq. 9,

$$k_f = k_f^0\exp\left(\frac{-\sigma_{ts}(x_m-\gamma)^2}{2k_B T}\right), \tag{8}$$

$$k_r = k_r^0\exp\left(\frac{(\sigma-\sigma_{ts})(x_m-\gamma)^2}{2k_B T}\right), \tag{9}$$

where k_f is the rate of bond formation, k_f^0 is the intrinsic rate of bond formation, k_r is the rate of bond breakage, k_r^0 is the intrinsic rate of bond breakage, σ is the spring constant of the bond, σ_{ts} is the transition-state spring constant, x_m is the length of the bond, γ is the equilibrium length of the bond, k_B is the Boltzmann constant, and T is the temperature.

For each receptor-ligand pair, a uniformly distributed random number is compared to the probability given by $P(\Delta t) = 1 - \exp(-k_f\Delta t)$ for bond formation. If this random number is less than the probability, then a bond between the receptor and ligand is formed. The analogous calculation is performed for bond breakage for any existing bonds using the rate of bond

breakage, k_r; $P(\Delta t) = 1 - \exp(-k_r \Delta t)$. The pseudo-random numbers used throughout our implementation of this algorithm are generated by the Mersenne twister algorithm (27).

The force that the bond exerts on the viral particle is calculated by modeling each bond as Rouse-like springs (see below). The compression or extension of the spring gives a restoring force that is summed with the other extrinsic forces in each time step of the Ermak and McCammon algorithm (23).

Coarse-grained *env* trimers

We employed a modified Rouse polymer model (28) to coarse-grain the trimeric structure of the *env* protein stalk. As our focus is the interaction of gp120 and CD4, we modeled gp120 trimers as a set of three bead-spring units attached to a fourth bead-spring (which represents the single gp41 stalk (29)). The free bead-spring units represent individual gp120 monomers and each can form a bond with CD4. The gp120 bead-springs are free to move in all directions, though there are interparticle steric forces keeping two beads from colliding. The value of the repulsive radius surrounding each gp120 is 5 nm, which is in agreement with crystal structure data of the bound gp120-CD4 complex (4) and other measurements of the gp120 structure (11,13,22,30). The gp41 stalk is always kept normal to the virus to simplify the force calculations in each time step, and hence the force on the virus is due to the stretching of the gp41 stalk, as collectively driven by the actions of the trimer. We model the location of gp41 as fixed on the viral envelope.

Coarse-graining allows for relatively high resolution and large time step calculations of the binding of HIV to a cell surface. Ultimately, more structural detail can be added to the model by incorporating separate domains of gp120 as individual bead-springs. One important future extension will be the inclusion of a separate binding site for the chemokine coreceptor. A representative schematic of the system with gp120 trimers expressed on the virus is shown in Fig. 1.

Protein diffusion

Cellular receptors are mobile on the cell surface (31). In our simulation, the receptors in the plane are modeled as single disks that can form bonds with the terminal bead of a gp120 monomer. To investigate the role of protein diffusion on the degree of binding of the virus to the cell surface, we allow the cellular receptors to diffuse laterally. This motion is calculated by solving the Langevin equation for each receptor using an algorithm due to Ermak and McCammon (23) with identities shown in Eqs. 1–3. Since the cell membrane in our model does not deform, we restrict diffusion of the receptors orthogonal to the plane of the membrane. Therefore, we only calculate the diffusion of the proteins in two dimensions. The random walk of the individual proteins produces expected values of the mean-squared displacement over long times. The diffusion constant of CD4 bound to gp120 in the cellular membrane has been measured as 5×10^{-10} cm^2/s (31). We use this value for the diffusion constant to calculate the two-dimensional diffusion of both bound and unbound cellular receptors, as well as the drag force on bound receptors. When a gp120 molecule is bound to CD4, it can induce a lateral force that will affect the molecule's motion in tandem with thermal motion. We assume that the force on the protein cannot deform the cell membrane, so we are concerned only with the motion of the protein in the plane of the membrane. Every receptor experiences Brownian motion during each time step.

We do not track diffusion of the cellular receptors before the virus first forms a bond with the surface to limit computational time. We model a region

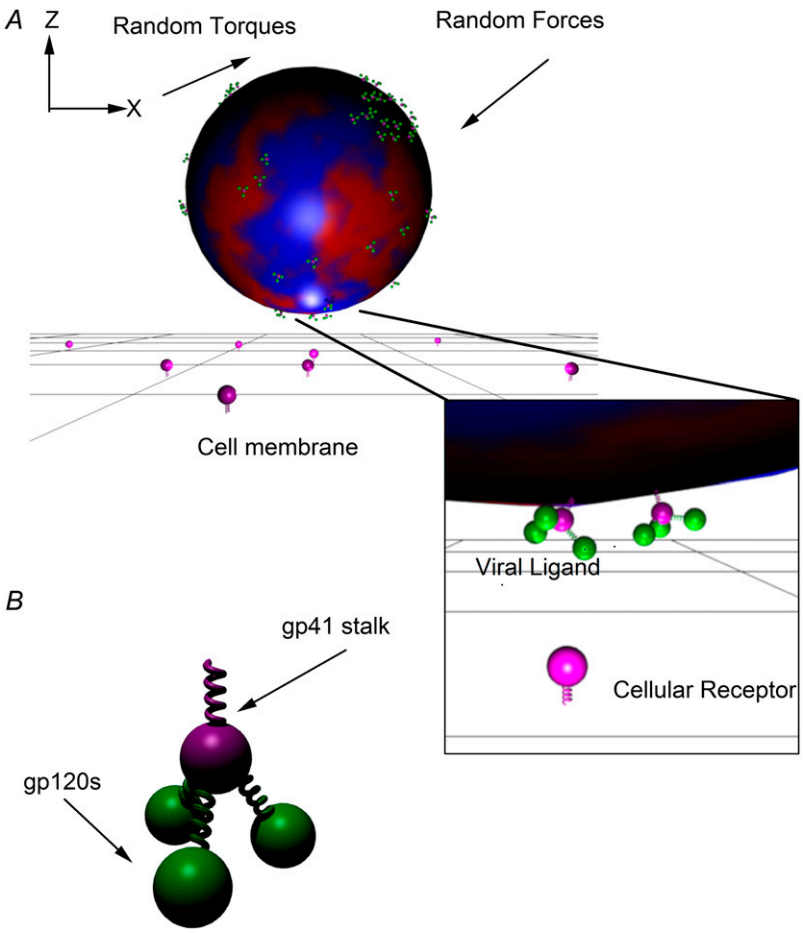

FIGURE 1 Schematic of Brownian adhesive dynamics viral-cell interactions. (*A*) Solid viral sphere in a coordinate system with relation to the cellular surface along with the random forces and torques acting on the virion. The *env* trimers are randomly distributed on the viral surface. These proteins interact with CD4 receptors in the plane of the cell membrane. (*B*) Construct of the modified Rouse polymer bead-spring model of *env* trimers used in the simulation.

of the cell surface 10 viral diameters of the cell membrane and, to ensure stable local densities of receptors, the edges of this region of the cell surface connect as a repeating lattice. As an example of this reflecting boundary condition, a receptor diffusing off the southwest edge of the modeled area will reappear on the northeast edge. The volume of the cellular receptors was modeled as a single point on the cell surface. We did not include any method of avoiding cellular receptor overlap as the receptors diffuse on the cell membrane. Once the cellular receptors are bound to gp120, the repulsive diameter of gp120 keeps the molecules apart. Including lateral repulsive forces on cellular receptors may be important in future calculations where the receptor density in the contact zone reaches the packing limit.

Adaptive time step

To investigate the role of cellular receptor diffusion on the steady-state configurations of viral bonds in tractable computational time, we employ an adaptive time step in our algorithm. When the virus is unbound, a small time step is used as prescribed by the propagation algorithm of Ermak and McCammon (23). Once the virus forms a bond, the contact zone is interrogated for any unbound proteins. The contact zone for the tethered virus changes as the separation distance between the virus and the cellular membrane changes due to the thermal motion of the virus.

To determine which viral proteins should be included in the contact zone, we performed an analysis of the probability of bond formation used in the Monte Carlo scheme at varying distances from the cell surface. We do not consider any viral proteins that have a probability of bond formation $<10^{-6}$ as being in the contact zone. Our truncation of the probability density function introduces an error of $<0.01\%$ in the cumulative probability of bond formation. We only interrogate gp120 trimers for binding that are stretched or compressed a maximum of 3.2 nm from the equilibrium bond length (roughly 22% of the equilibrium bond length). Using the transition-state spring constant of 1.1×10^{-1} N/m, the limit of 3.2 nm excludes any trimers that have a probability of bond formation of $<10^{-6}$.

If there are no available unbound viral or cellular proteins in the contact zone, the algorithm switches to employing a long time step (10 ms). During long time steps, we assume that the virus and bound cellular receptors do not diffuse. This heuristic is based on the assumption that the bonds tethering the virus to the cell surface will reach an equilibrium length on the timescale of the long time step. For each long time step we still calculate the thermally driven rotation of the virus to ensure that the contact area is completely interrogated. This also allows the virus to relax along the three rotational degrees of freedom.

The diffusion of all unbound cellular receptors in the field is calculated for each long time step. During each long time step, we use the unstressed off-rate to calculate the cumulative probability that a bond will dissociate. Once a bond breaks, or an unbound cellular receptor diffuses into the contact zone while there are still unbound gp120 monomers in the contact zone, the algorithm reverts to the short time step. For short time steps, the microscopic details of bond formation and dissociation are calculated at each time step as before. This adaptive time step algorithm has increased the tractable range of simulation time from fractions of seconds to minutes.

Calculation of the rate constant of particle binding

To calculate the rate constant of binding of the virus to the cell surface, we utilize the algorithm of Northrup et al. (32). The overall rate constant for viral docking is constructed from three driving probabilities: the probability that the virus will bind when it is in close proximity to the cell surface; the probability of the virus escaping from the cell surface; and the probability of the virus returning to the surface after unsuccessful binding (32). Each of these probabilities can be measured in simulations and are used to calculate the overall rate constant for viral binding given by Eq. 10,

$$k_v = \frac{k_D\left[\frac{\beta}{1-(1-\beta)\Omega}\right]\alpha}{1-(1-\alpha)\left\{\Delta + \left[\frac{\beta}{1-(1-\beta)\Omega}\right](1-\Delta)\right\}}, \quad (10)$$

where k_v is the binding rate constant, $k_D(b)$ is the diffusion rate constant near the cell surface, α is the probability that a collision will lead to viral binding, β is the probability that a bond will form when the virus is close to the cell surface, Ω is the probability that a virus diffusing to an outside boundary will return to the starting position, and Δ is the probability that a virus that does not bind when it encounters the cell will interrogate the cell surface rather than diffuse back to the starting position. Each of these probabilities can be calculated or estimated from solution of the diffusion equation. Thus, by calculating the probability of virus binding, β, we can calculate the rate constant of viral docking, k_v.

Model parameters

The physical parameters used in the computer simulation are motivated by those measured for HIV and are summarized in Table 1. The value for the binding and dissociation rates were calculated as previously described (14,15). The spring constant is not available for the gp120-CD4 interaction, so we use spring constants consistent with other protein-protein interactions (29). We have assessed through separate calculations that the effect of the spring constant on virus binding, and the average number of bonds formed, is negligible, even with a change in the compliance as much as 50% (14). To model the microscopic events leading to bond formation and dissociation, we use a short time step of 1 ns and a long time step of 10 ms. The short time step is sufficiently long so that $\Delta t \gg \mathbf{MD}/k_BT$ and short enough that the restoring force on the virus during a single time step is nearly constant. These boundaries are prescribed by Ermak and McCammon (23). The long time step is sufficiently small that the probability that a bond will dissociate in a single time step is small, while it is large enough that the calculation of the bond configuration over long timescales becomes computationally tractable.

RESULTS

Fig. 2 *A* shows a typical simulated trajectory of viral motion. The virus begins at the origin (located a viral diameter, 90 nm, away from the cell surface) and then undergoes a three-dimensional random walk until it comes into molecular contact with the cell surface. In the trajectory illustrated in Fig. 2 *A*, the virus moves about one viral radius before the first bond is formed. Once a bond is formed, the virus becomes tethered to the cell surface and there is a rapid increase in the total bond number (Fig. 2 *B*).

TABLE 1 Physical parameters used in BM-AD

Parameter	Value	Reference
Virus diameter	90 nm	(21)
Unstressed bond length	14.3 nm	(14)
Bond spring constant	1.2×10^{-1} N/m	(29)
Transition-state spring constant	1.1×10^{-1} N/m	(29)
Cellular receptor density	12,000 mol/cell	(46)
Cellular receptor diffusion constant	5×10^{-10} cm^2/s	(31)
k_f^0	6.72×10^4 M^{-1}s^{-1}	(37)
k_r^0	1.5×10^{-3} s^{-1}	(37)
Δt	1 ns	Calculated
Adaptive Δt	10 ms	Calculated

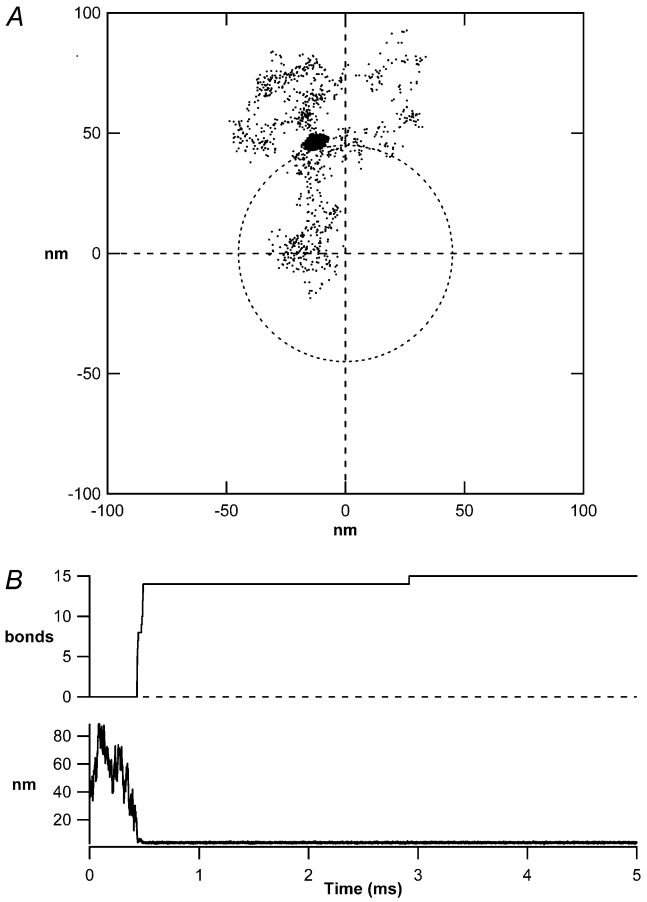

FIGURE 2 Sample trajectory of viral binding simulation. (*A*) The projection of the centroid of the virus onto the *xy* plane of the cell surface. The trajectory begins at the origin of the graph and the viral diameter is projected on the plane and indicated by the dashed circle centered at the origin. In the first 0.5 ms of random motion, the virus searched a space of ~1 viral diameter (90 nm). (*B*) The separation between the cell membrane and the viral envelope along the *z* axis and the number of bonds versus time.

Effect of gp120 trimerization on the rate of viral attachment

We first investigate the role of gp120 spike density on the probability of binding and the calculated binding rate constant. Using the algorithm of Northrup et al., we calculate the binding rate constant of viruses expressing a single *env* spike binding to surfaces with varying CD4 densities (32). To understand the effect of gp120 trimerization on viral binding, we compare the results calculated with the homotrimer of gp120 using our Rouse-like model to that when gp120 is modeled as a single spike, as was done previously (14,33). Fig. 3 shows the differences in the binding probability and the calculated rate constant shown with the different models. Viruses binding with gp120 trimers demonstrated significantly greater binding rate constants when binding to surfaces with 8×10^9 CD4/cell ($t = 4.02$, $df = 44000$, $p < 0.001$); 4×10^9 CD4/cell ($t = 4.99$, $df = 52010$, $p < 0.001$); 2×10^9 CD4/cell ($t = 4.54$, $df = 100{,}000$, $p < 0.001$); 1×10^9 CD4/cell ($t = 2.23$, $df = 100{,}000$, $p < 0.05$); and 500×10^6 CD4/cell ($t = 2.26$, $df = 100{,}000$, $p < 0.05$) than viruses expressing the single-spike model. (These CD4 densities were selected to make a direct comparison with English and Hammer (14); other calculations in this work were performed at 12,000 CD4/cell, unless noted). The increased binding probability and subsequent increase in the binding rate constant is due to the increased number of gp120 monomers in the localized area of the *env* spike.

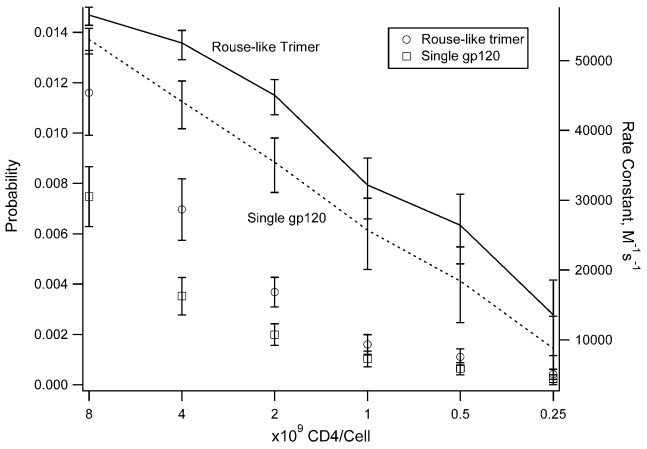

FIGURE 3 Comparison of trimerized gp120 model with single gp120 spike. The calculated binding rate constant is shown for model viruses with a single *env* spike interacting with surfaces with different CD4 densities by the connected graphs. The two sets of data represent either a single binding node or the Rouse-like trimer model of gp120 for each *env* spike. The values of the binding rate constant are shown on the secondary axis. The symbols represent the probability that a collision will result in a binding event for these same viruses, with the values depicted on the primary axis. Each point represents the mean of at least 40,000 simulations and the error bars represent the 95% confidence interval for that data point. Despite the overlapping 95% confidence intervals for trials on the surfaces with few CD4 particles (1×10^9 CD4/cell or fewer), using ANOVA, we find that the changes in CD4 and in the trimerized *env* model produce significant changes ($f(11{,}600{,}000) = 111.22$, $p < 0.001$). Furthermore, using the paired *t*-test, the difference caused by the trimer model in rate and binding probability for viruses binding to 8×10^9 CD4/cell ($t = 4.02$, $df = 44{,}000$, $p < 0.001$), 4×10^9 CD4/cell ($t = 4.99$, $df = 52{,}010$, $p < 0.001$), 2×10^9 CD4/cell ($t = 4.54$, $df = 100{,}000$, $p < 0.001$), 1×10^9 CD4/cell ($t = 2.23$, $df = 100{,}000$, $p < 0.05$), and 500×10^6 CD4/cell ($t = 2.26$, $df = 100{,}000$, $p < 0.05$) are significant. The difference seen for the viruses binding to surfaces with 250×10^6 CD4/cell had a $p > 0.05$.

Effect of CD4 diffusion in the cell membrane on degree of binding

In our previous computer experiments, when viruses bound to cells with a high density of CD4 that was fixed to the surface, only a few bonds were formed (14). Using a physiological CD4 density, if CD4 is fixed on the cell surface, there is an increase in bond number until all of the free CD4 in the contact zone are bound to gp120. In the absence of diffusion of CD4, and for typical densities of CD4 on the cell surface, if more than a single *env* trimer is in the contact zone, the CD4 density will limit the ability of the virus to engage all of the gp120 molecules in the contact zone. However, CD4 diffuses

(34) and we investigate the implications of its diffusivity on the degree of binding achieved by HIV to cell membranes. Over a long time, the level of binding that a virus can achieve is clearly dependent upon the diffusion of the CD4 molecules in the cellular membrane and the lifetime of the tether of the virus to the cell membrane. Once a bond with the surface is formed, the gp120 molecules on the viral surface act as a sink for CD4 receptors that diffuse into the contact zone. We calculate from the diffusion constant of CD4 (1×10^{-14} m^2/s), the density used in our simulation (4×10^{-9} CD4/cm^2), and the contact diameter of the virus that the average time for a new free CD4 receptor to diffuse to the edge of the contact zone is 2.5 s. Thus, on this timescale or longer, receptor diffusion should lead to an accumulation of binding sites into the contact zone.

However, it is also possible that lateral diffusion of CD4 may assist binding on a shorter timescale, as it may facilitate proper orientation of CD4 and gp120. Therefore, we have also examined the effect of lateral motion on binding over shorter timescales before receptors could accumulate in the contact zone. A comparison of the bond number after 0.1 s of virus binding to surfaces with fixed CD4 or diffusible CD4 is shown in Fig. 4. The mean number of bonds is larger when CD4 undergoes lateral diffusion than when it is fixed ($t = 3.81$, $df = 105$, $p < 0.001$). Likewise, CD4 diffusion leads to more gp120 trimers being fully engaged (Fig. 4 *B*, $t = 2.24$, $df = 105$, $p < 0.05$). Since there is more binding on this timescale with diffusion, these results indicate that local CD4 motion allows CD4 to find a more favorable configuration for binding, leading to more robust binding, even before widespread accumulation of CD4 into the contact zone.

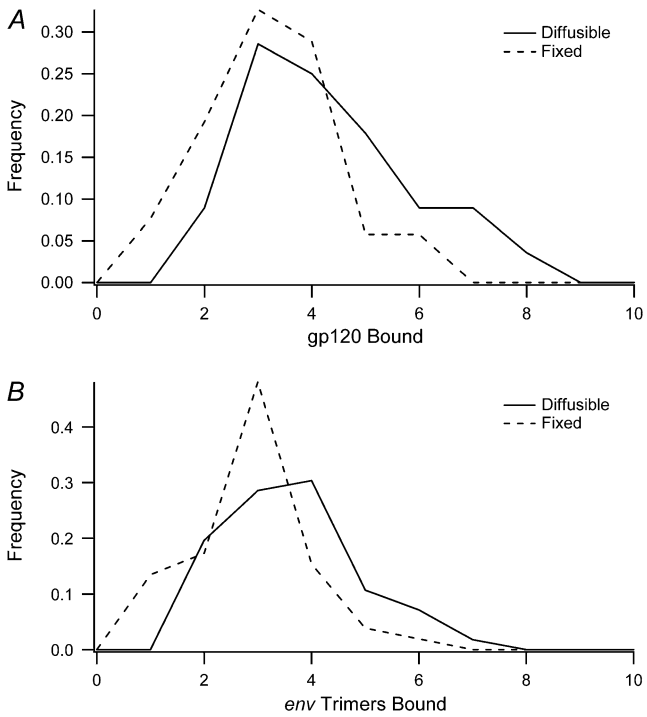

FIGURE 4 Distribution of bond number and number of gp120 trimers bound at 0.1 s. (*A*) depicts the distribution of bond number achieved for viruses expressing 72 *env* trimers interacting with CD4 surfaces that have either diffusible or fixed receptors after 0.1 s of simulation. (*B*) Distribution of individual protein spikes involved for the same trajectories as in panel *A*.

Fig. 5 illustrates the probability of a single bond breaking versus the number of bonds formed by the virus within 0.1 s of simulation. The probability of bond breakage is lower when the receptors can diffuse in the cell membrane than when they are fixed. The difference in mean probability of breakage is significant for each level of binding denoted with an asterisk ($p < 0.05$). Receptor diffusion facilitates the maintenance of bonds since CD4 motility allows the bond to relax more readily than when the attachment point is fixed to the cell surface. In Fig. 5, the probability of bond breakage is not reported for higher bond numbers since relatively few viruses interacting with fixed CD4 molecules achieve larger numbers of bonds.

Virus binding at steady state

Using our adaptive time step algorithm, we investigate the degree of binding achieved by viruses at steady state. We extend the timescale of the previous calculations reported in this article by at least three orders of magnitude to investigate the bond configuration after the virus interacts with the cells for tens of seconds—sufficient time for receptors to diffuse in the contact zone. For long times, we anticipate that CD4 accumulation in the contact zone will significantly increase the degree of binding for viruses with higher gp120 densities. For viruses with up to seven *env* trimers in the contact zone, we simulated viral docking until the binding reaches steady state.

In performing many simulations, we uncovered several general principles. We found that in each of our long timescale simulations, all of the gp120s in the contact area ulti-

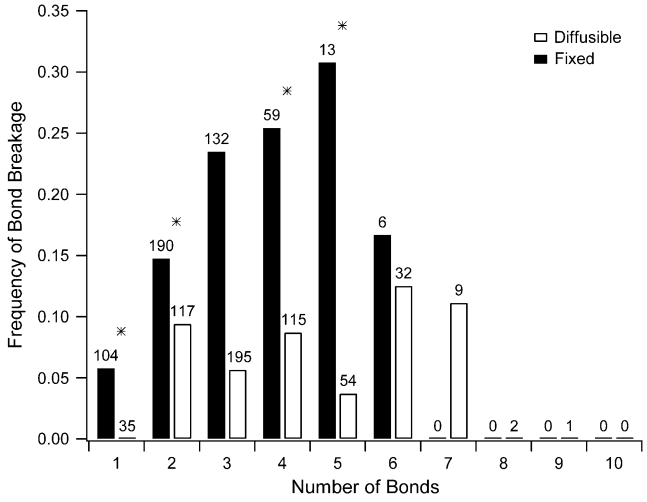

FIGURE 5 Frequency of bond breakage versus total number of bonds at 0.1 s. The percentage of viruses with at least a single broken bond are shown versus the total number of bonds achieved at 0.1 s of simulation for viruses expressing between 1 and 72 *env* spikes. The total number of simulations included in the frequency calculation is shown above the bar. An asterisk above a bar indicates a significant difference between fixed and diffusible viruses with $p < 0.05$.

mately become fully engaged to CD4. Furthermore, we find that after a single bond dissociates, an unassociated gp120 often rapidly binds to a free CD4 once again.

Our steady-state calculations were limited to viruses with seven or fewer trimers in the contact zone. This was done to avoid the limit where bond crossover was possible, to correspond to what is generally accepted to be the average gp120 architecture (13,22) and to limit computational time. Specifically, we can relate the gp120 density to the probability of bond overlap. In our model, the *env* stalk is free to pivot on its viral attachment point along all three degrees of freedom unhindered. We can use this to map out the potential volume that each individual *env* spike can occupy around the viral surface. Utilizing work done to calculate the closest packing of circles on a sphere (35), we see that with no limitation to the *env* rotation, at most 32 *env* trimers can be placed on the viral envelope ensuring no bond overlap.

If *env* spikes are not permitted to rotate away from the normal, the maximum number of bonds that can be packed onto the viral surface will be increased. By permitting *env* molecules to tilt 45° from the normal, the most efficient packing of *env* spikes would allow 73 spikes on the envelope with no overlap (Fig. 6 *B*). Conversely, if the *env* stalks are free to rotate, we calculated that no more than seven trimers can interact with a planar surface without overlap.

Thus to avoid overlapping of bonds, we calculate the steady-state binding for viruses with seven or fewer *env* trimers in the contact zone. We find that for these viruses, all gp120 trimers in the contact zone are fully bound to CD4 given enough time. Fig. 7 depicts the elapsed time before all of the viral proteins become fully engaged. As the number of gp120 trimers in the contact zone increases, the time until all trimers are fully engaged increases.

We also investigate the time for trimers of gp120 to be fully engaged—where each of its gp120 arms is bound to a CD4 molecule. Structural evidence indicates that after binding of gp120 with CD4, the gp120-CD4 complex moves away from gp41 and a cryptic binding site for chemokine receptor is revealed. For certain viral strains, all three gp120 monomers of a single *env* spike must be bound to CD4 to support its dissociation from gp41 (5). Thus, we need to assess the probability of forming fully engaged trimers to assess the probability of eventual fusion and infection. The average time before a single gp120 trimer becomes fully engaged to CD4 is shown in Fig. 7. We see that time elapsed before a single gp120 trimer is fully bound to CD4 increases slightly as the number of gp120 trimers in the contact area increases. This trend can be explained by the increased likelihood of CD4 binding to gp120 molecules on different *env* spikes initially when there are more spikes in the contact area. Also, it can take many seconds for all the gp120s to be fully engaged.

CD4 receptor configuration at steady state

We examine the configuration of bonds as CD4 receptors diffuse and bind in the contact area. Fig. 8 depicts the relative positions of cellular receptors and their binding state over the course of a simulation for a representative virus with five *env* trimers in the contact area. There is an initial rapid increase of binding followed by a slower phase which is limited by the

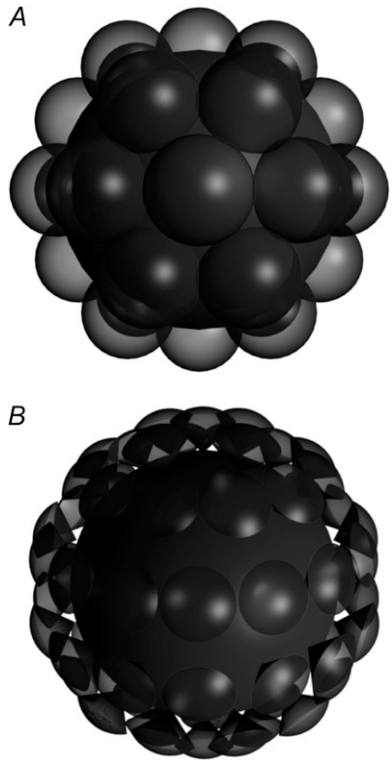

FIGURE 6 Volumes of possible bond formation for each *env* spike. The volume that a single *env* spike can occupy is shown on the viral surface. (*A*) Rotational degrees of freedom are not limited, so the volume is a complete hemisphere shown on the surface of the virus. The most efficient packing of these volumes results in a maximum of 32 *env* spikes on the surface of the virus as shown. (*B*) Volume of each *env* spike with a limitation of 45° from normal to the viral surface. The efficient packing of these volumes results in a maximum of 73 nonoverlapping *env* spikes on the surface of the virus.

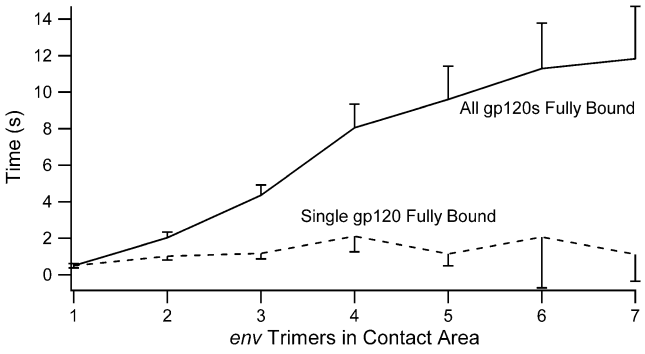

FIGURE 7 Adaptive time step calculation of time to reach steady-state binding and time before a single gp120 trimer becomes fully engaged to CD4. The time elapsed before all gp120s in the contact zone are fully bound to CD4 is shown with the solid line. The time before a single gp120 trimer becomes fully engaged to CD4 is shown with the dashed line. Each error bar depicts the 95% confidence interval for that point.

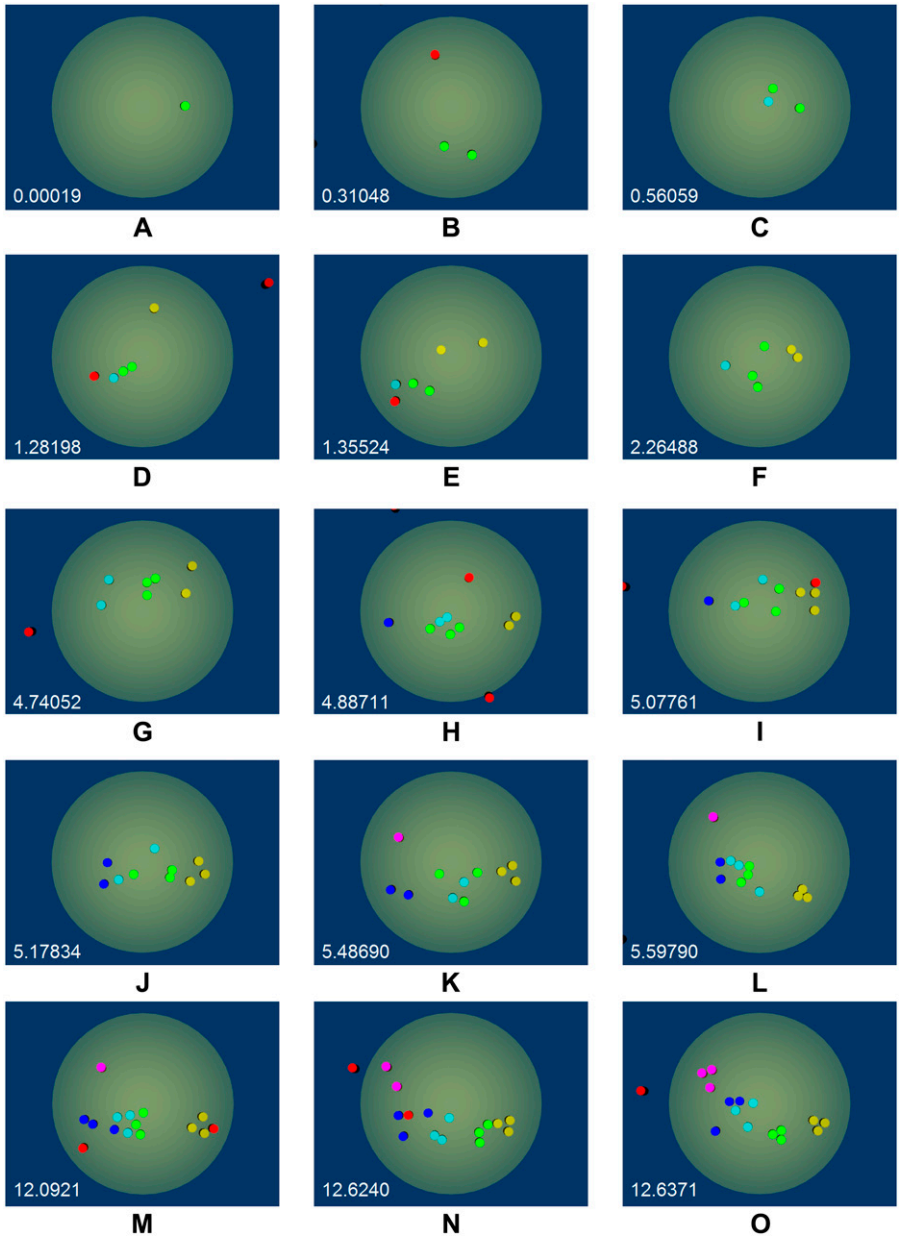

FIGURE 8 CD4 receptor configuration time-course. The progressive accumulation of CD4 molecules under the virus is shown for a virus with five *env* spikes in the contact zone binding to steady-state with all *env* spikes in the contact zone fully bound. The shadow of the virus as projected on the plane of the cell surface is shown as the green circle. The smaller dots indicate a single CD4 molecule. Red CD4s are unbound, while the colors of the bound CD4s indicate binding to a common *env* spike. The total time elapsed in the simulation is indicated in the lower left portion of each panel. Two events of bond breakage and reformation between panels (*L*) and (*M*) are not shown in the time-course. Only after the rearrangement of the CD4 proteins in the contact area are the CD4s attached to a single *env* trimer in a ''tight'' configuration.

diffusion of CD4 into the contact zone. As the simulation progresses, there is an accumulation of CD4 in the contact area and, between binding events, the CD4 receptors change their relative configurations. This receptor motion is driven by both the thermal diffusion of the bound receptors as well as the force from the bond which acts to drag individual receptor to new locations.

The representative example shown in Fig. 8 illustrates that even with a total of five *env* trimers available for binding in the contact area, the initial binding events involve several different viral spikes. These initial bonds tether the virus, until other CD4 molecules accumulate within the contact zone. When trimers are first fully engaged, gp120 molecules from the same trimer are engaged over a distance. Ultimately, as the simulation progresses, the trimers become ''tight'', as the engaged CD4 for each trimer are tightly clustered under each *env*. If fully engaged trimers in a ''tight'' configuration are required for viral entry, then the time to form these tight trimers may help explain why viral entry can take seconds or longer (36), when binding rapidly occurs within fractions of a second.

Effect of gp120 density on pseudo steady-state binding

We investigate the configuration of binding sites over a short timescale of 0.1 s using a time step of 1 ns. By simulating the diffusion of the virus and proteins and the probability of bond formation and breakage, we can determine the fine details of

bond formation and breakage for initial times. Over this short timescale, we generally find that binding reaches a pseudo steady state, where all CD4 molecules initially in the contact zone are bound, before the diffusive accumulation of receptors in the contact zone.

We simulated the effect of CD4 diffusion on the number of bonds formed within 0.1 s as a function of total viral *env* trimer density as shown in Fig. 9. Clearly, the level of binding increases with increasing number of *env* molecules. CD4 diffusion increases the average level of binding achieved at all gp120 densities simulated, even for short times. However, the number of fully bound gp120 trimers increases with CD4 diffusion only if the density of gp120 molecules on the virus is high. Presumably, at low gp120 densities, sufficient CD4 is available without diffusion to rapidly form bonds to all unbound gp120 trimers in the contact zone. In simulations of viruses with low gp120 densities (expressing only one or two *env* spikes in the contact area), most viruses will have at least one gp120 fully engaged to three CD4 molecules by 0.1 s. However, at high gp120 densities, competition between gp120 molecules for available CD4 means that CD4 diffusion is necessary to overcome competition and allow CD4 molecules to associate with gp120 to form fully engaged trimers.

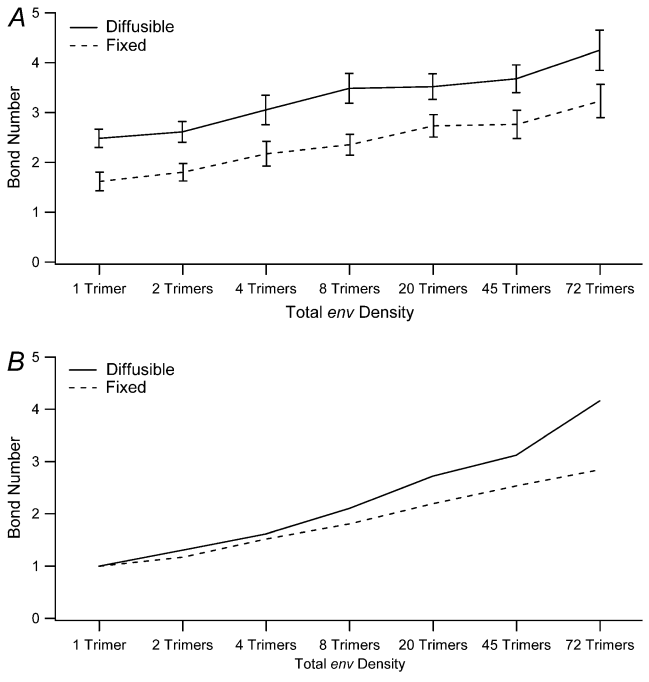

FIGURE 9 Degree of binding with diffusible and fixed CD4 at 0.1 s. (*A*) Number of bonds formed after 0.1 s of simulation with viruses expressing varying densities of gp120. The solid line represents binding with diffusible CD4 receptors. The dashed line represents viruses interacting with fixed CD4. The bars depict the 95% confidence interval for each point. The difference between diffusible and fixed CD4 for all points is significant with $p < 0.005$. (*B*) The number of trimers bound at 0.1 s for each of the trajectories. The difference between fixed and diffusible CD4 are significant with $p < 0.005$ only for viral *env* densities of 8 and greater.

Effect of gp120 density on binding probability and rate constants

There is some debate about the number of *env* trimers that are necessary for optimal viral binding and entry. It has been shown that a single *env* homotrimer is sufficient to cause viral fusion (8), indicating that a single spike can form a fusion pore once fully bound to CD4. This result suggests that only a single gp120 trimer may be necessary for viral entry. However, we question how the rate of viral binding might depend on gp120 timer density, or alternatively, what the optimal density is to maximize binding and the formation of fully engaged trimers. To elucidate the role of gp120 density on the kinetics of binding, we calculate the kinetic rate constant of virus binding with different densities of gp120 spikes using the algorithm of Northrup et al. (32). The results of these calculations are shown in Fig. 10 *A*.

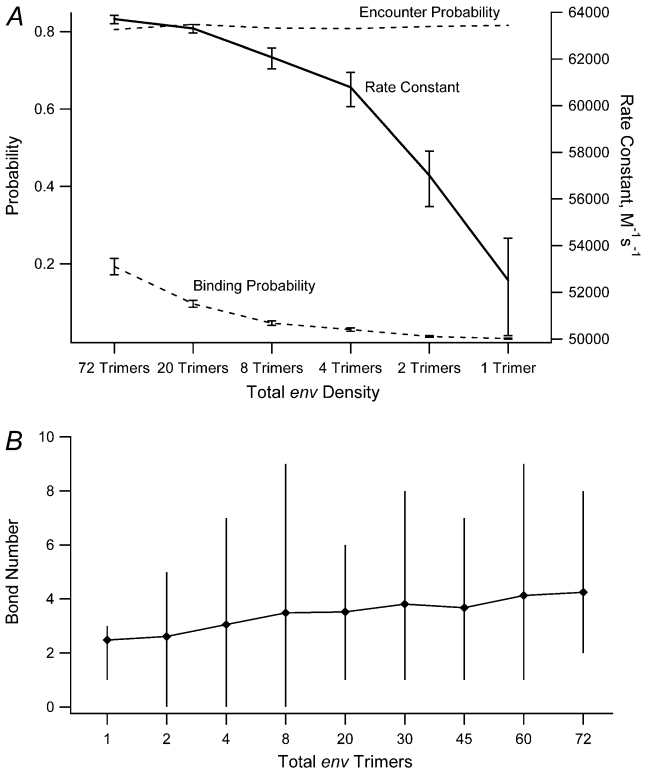

FIGURE 10 Binding rate constant and mean bond number after 0.1 s for varying *env* trimer densities. A number of probabilities were measured for a virus starting at a viral diameter (90 nm) separated from the cell surface to calculate the binding rate constant using the method of Northrup et al. (32). Two of these probabilities, the probability of the virus encountering the cell and whether the virus forms a bond with the cell, for different gp120 densities are shown in panel *A* as dashed lines. The calculated binding rate constant is depicted as the solid line with values shown on the secondary axis. The vertical bars at each point represent the 95% confidence interval for that point. ANOVA analysis of this data indicates these values are significantly different ($f(561,050) = 530$, $p < 0.001$). (*B*) Mean number of bonds achieved at 0.1 s of simulation for 100 viruses with different gp120 densities. The diamonds depict the mean value while the bars show the range of values from low to high for each set of trajectories.

We performed simulations of viral docking by starting the virus 90 nm above the cell surface and running the simulation until the virus either binds, diffuses to 230 nm above the cell, or comes within a bond length of the cell surface and diffuses back to the starting position. The solid line in Fig. 10 *A* depicts the kinetic rate constant of binding of viruses with different densities of gp120. For high gp120 densities, the rate constant for viral binding is independent of gp120 density; there is only a 2.5% reduction in the binding rate constant when the total number of trimers is reduced from 72 to 8. The rate constant of viral binding drops as the number of gp120 trimers is reduced to <8 on the viral surface. These results indicate that viruses with as few as eight *env* spikes will bind nearly as quickly to CD4 surfaces as those with 72 spikes. Furthermore, the maximum calculated rate constant of 64,000 $M^{-1}s^{-1}$ is within 5% of that measured by surface plasmon resonance of 67,200 $M^{-1}s^{-1}$ for HIV binding to a CD4 substrate (37).

Our calculations show a significant drop in the binding rate constant for viruses with fewer than eight *env* trimers. To determine whether this lower rate of binding is caused by the lower probability that these viruses will display an *env* spike oriented toward the cell surface, we estimated, using the average length of the gp120-CD4 bond (14.3 nm), that the initial contact zone on the viral surface covers ~13% of the surface area of the virus. Since the proteins are uniformly distributed on the viral surface, viruses with eight or more trimers are likely to express a trimer in the 13% of the surface involved in binding. Using the Poisson distribution, we show the probability of at least a single gp120 in the initial contact area for varying total viral *env* trimer density in Fig. 11. With a total trimer density of <8, there is a higher probability that the virus will not express a trimer in the area initially presented to the cell surface. There is a $>50\%$ chance for a single *env* spike in the contact area when the virus expresses >3 *env* in total. At these low gp120 densities, then, binding is affected by the rate of CD4/gp120 encounter.

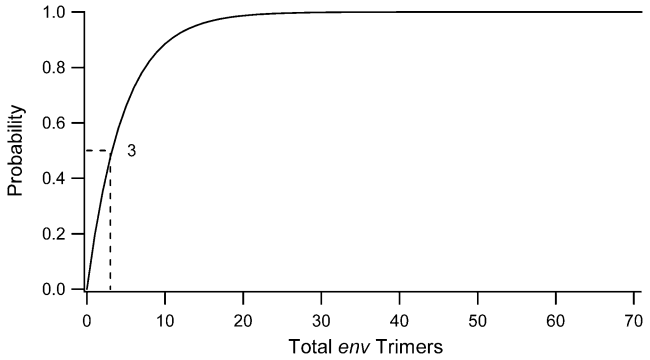

FIGURE 11 Poisson distribution of the probability of at least a single *env* spike in the contact area. We calculate the probability that the virus will have at least a single trimer within the contact zone for varying total densities of *env*. For viruses with >3 *env* spikes, the probability is $>50\%$ that there will be a trimer in the contact zone. The probability that there is at least a single spike in the contact zone approaches 1 for total *env* densities of over 20.

Effect of gp120 density on fully engaging a single *env* spike

Assuming that a single fully engaged gp120 trimer is sufficient to form a fusogenic pore, we investigate the effect of gp120 density on the likelihood a virus will have a fully bound trimer spike during a 0.1 s encounter. As we showed, the system does not reach steady state on this timescale, but we are interested in the binding configuration at pseudo steady state, after initial binding has rapidly equilibrated, and the limiting CD4 in the contact area has interacted with the virus. Our previous calculations have shown that all *env* trimers in the contact area will be fully bound once the viral simulation is allowed to reach the true steady state (and every *env* in the contact zone will be trimerically bound). Thus, it is more relevant to ask what the kinetics of bound trimer formation might be.

For short timescales, while the probability of docking increases as the number of gp120 trimers increases (Fig. 9), the probability that a single trimer will be simultaneously bound to three CD4s decreases as the gp120 density increases. Since the cell has a low local concentration of CD4 in the contact zone, each free gp120 must compete for the limited CD4 in the contact zone. Correspondingly, there must be an optimal density of *env* trimers that maximizes the probability of fully bound trimers on the short timescale, before reaching the diffusion-limited regime of viral binding. In Fig. 12, the dashed lines depict the probability of virus binding and the probability that at least a single trimer becomes fully engaged at pseudo steady state (0.1 s). The product of these two probabilities, shown with the solid line in Fig. 12, represents the probability that a virus encountering the cell surface will have a fully engaged trimer. We call this metric the ''efficiency'' of viral entry, presuming that a trimer must be fully engaged to secure entry.

We find that efficiency is maximized when viruses have 13 gp120 trimers when binding to cells expressing ~12,000 CD4/cell. There is a sharp increase in the efficiency as the density of gp120 increases from 1 to 13, beyond which the efficiency decreases. At low gp120 densities, the low probability that the virus will form a bond with the cell surface constrains the efficiency. At higher gp120 densities, competition among gp120 molecules leads to a lower probability of achieving a fully engaged trimer and constrains the efficiency, as gp120 molecules compete for unbound CD4 molecules in the contact zone.

Effect of CD4 density on binding rate constant and achieving a single fully bound *env* spike

The calculation of the binding rate constant is dependent upon the density of cellular receptors in the contact zone. For cells that express ~12,000 CD4/cell, there are initially ~3 CD4s per viral contact area, so we anticipate that the binding rate constant is dependent on CD4 concentration. We extend

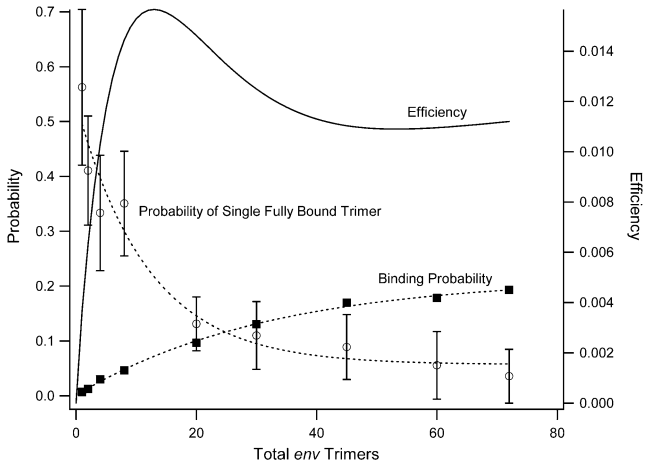

FIGURE 12 Binding probability, frequency of fusogenic bond formation, and efficiency. The probability of viral docking measured in simulation is shown for viruses with varying densities of gp120 trimers as the solid boxes. An exponential fit to these data is shown as the dashed line. The probability of at least a single trimer being fully engaged is depicted at each density of gp120 with the open circles. The vertical bars depict the 95% confidence interval for each gp120 density. The associated exponential fit is shown as the dashed line. The multiplication of these two functions is the surrogate for efficiency of fusogenic bond formation and is shown as the solid line. The values for the efficiency are shown on the secondary axis. The peak value is seen for a total *env* density of 13 spikes.

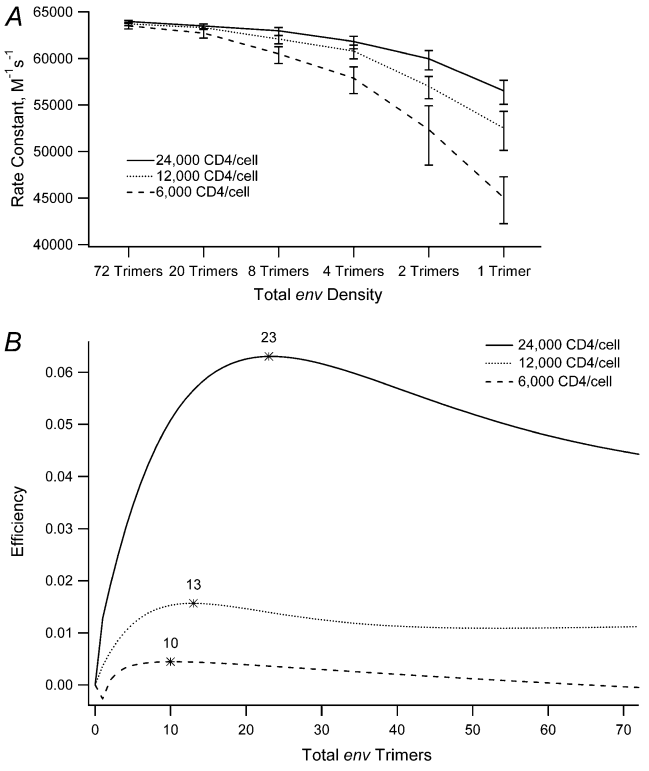

FIGURE 13 Binding rate constants and efficiency of forming trimers for different values of CD4 density. The binding rate constant (*A*) and fusogenic efficiency (*B*) of viruses binding to surfaces expressing a range of CD4 densities (~6500 CD4/cell, ~12,000 CD4/cell, and ~24,000 CD4/cell) are shown. Vertical bars indicate the 95% confidence interval for the values in panel *A*. The asterisks in panel *B* denote the peak value of the efficiency line and represent the gp120 density that optimally results in a trimer being fully engaged by CD4.

our previous calculations to determine the binding rate constant for viruses binding to surfaces as CD4 density is varied between ~6500 CD4/cell and ~24,000 CD4/cell.

Fig. 13 *A* illustrates that the rate constant for binding decreases as the gp120 density decreases at all CD4 densities. When the gp120 density is high, the rate constant for binding is independent of CD4 density. For example, when the CD4 density is 6500 CD4/cell, the binding rate constant for viruses with eight trimers is within 5% of the value calculated with 72 trimers. When the gp120 density is low, the rate constant for binding decreases sharply for low CD4 density. Furthermore, when the CD4 density is high (24,000 CD4/cell), the rate constant for binding is high and independent of gp120 density.

We also calculated the efficiency for short encounters as a function of CD4 density. Repeating the calculations of the efficiency of binding (the probability of binding multiplied by the probability of having a fully engaged trimer), we show there is always an ideal density of gp120 for every CD4 density. The peak efficiency falls between 10 and 23 gp120 trimers, and the ideal number of gp120 molecules increases as the CD4 density increases.

DISCUSSION

In this article, we have extended Brownian adhesive dynamics to deal with trimerized viral adhesion proteins, such as seen with *env* on HIV. Trimers were simulated using a Rouse-like polymer model of the trimer. Our simulations were used to determine the role that trimerization of gp120 has on the probability of virus-cell binding, and the kinetics and probability that trimers will be fully engaged during viral docking. First, we illustrated that trimers significantly increase the probability of bond formation and the binding rate constant compared to a single gp120 monomer.

We found that CD4 diffusion in the cell membrane increases the number of bonds formed between the virus and cell, both over short and long times. We estimate that within seconds, the diffusion of receptors into the contact zone will result in HIV fully engaging every gp120 trimer in the contact zone. However, we also illustrate that at short times, receptor diffusivity enhances binding. Our simulation results may explain some of the microscopic details leading to the lower infectivity of viruses in cells with hindered CD4 lateral diffusion (38–40). Without lateral diffusion, the gp120 trimers are less likely to reach a fully bound configuration and therefore less likely to infect the cell.

Our simulations determined the rate constant of binding as well as the configuration of bonds at 0.1 s, before significant receptor accumulation. We performed short timescale simulations to predict an optimal gp120 density to lead to a fully engaged gp120 trimer between the cell and surface at 0.1 s,

which can be viewed as a pseudo steady state, when the binding is at steady state but before the receptor accumulation has occurred. We also illustrated that there is always an ideal intermediate density of gp120 at which a single *env* trimer may be fully engaged.

The estimated number of *env* spikes on the viral surface has been debated. Ranges from two to 72 *env* trimers on wild-type viruses have been claimed (9–13). A study of the stoichiometry of *env* trimers indicated that a single homotrimer on the viral envelope is sufficient for the virus to infect a host cell (8). To understand the differences in binding of viruses with different expression levels of *env* spikes, we titrated the gp120 density on the viral envelope in our simulations to calculate the effect of gp120 density on the binding rate constant and the probability of forming a fully engaged trimer. We found that viruses with eight trimers bind to cell surfaces nearly as quickly as those with 72. As we increase the CD4 density on the surface, from ~12,000 CD4/cell to ~24,000 CD4/cell, the binding rate constant for viruses with fewer gp120 trimers increased while the rate constant for viruses expressing many trimers was unaffected. As the binding rate constant is dependent upon the contact frequency of gp120 and CD4, we see that increasing the CD4 density on the cell will increase the binding rate constant for viruses with few *env* spikes. These results could be corroborated with surface plasmon resonance measurements of HIV strains expressing different amounts of gp120 on surfaces bound with CD4 (37), though the total gp120 density on the viruses used in the surface plasmon resonance studies was not reported.

The events leading to HIV fusion and cellular infection occur on multiple timescales (36). In this simulation, we were concerned only with viral attachment. We performed simulations to a steady-state level and found that all available gp120 monomers were bound within seconds for viruses displaying between one and seven trimers in the contact zone. The amount of time elapsed between viral binding and infection has not been measured in vivo, but estimates indicate that the entire process of viral fusion after binding occurs on the order of minutes (36). While the initial binding can occur in a fraction of a second, the explanation for why fusion takes minutes is likely because the gp120-CD4 bonds must reconfigure in the interface to achieve full trimer engagement. Interestingly, when gp120 density is high, it takes longer for all the gp120 monomers to become fully engaged.

An interesting result from our simulations that may have implications for the timescale of viral entry is that fully engaged trimers where all of the CD4 molecules are clustered tightly around each *env* spike take some time (seconds) to form. This delay is due to the reorganization of the CD4 molecules through lateral diffusion to the lowest energy state. Although initial viral docking can take a fraction of a second, minutes are required for clustering the CD4 molecules tightly (36). Entry is known to take minutes to hours (36,41,42), and require not only trimerization but also engagement of chemokine receptors (43,44). However, the results shown here indicate that minutes may be required to organize CD4 molecules in the proper orientation for entry.

Entry must compete with viral inactivation. Work on the kinetics of viral entry demonstrate a measurable rate constant for viral inactivation once the virion is bound to the cell surface (41). Platt and co-workers measured the rate constant of inactivation at ~0.47/h and the rate of entry for fully formed complexes at ~0.09/h (41). More importantly, the percentages of attached viruses that eventually infect the cell were also calculated. For viruses infecting cells with a high coreceptor density (effectively the infectivity of these viruses was limited only by the gp120-CD4 interaction) only 15% of the attached viruses infected the cell. Other measurements of neutralization of bound virus indicate that competing effects limiting the ability of the virus to infect a cell occur on the order of minutes (41,42,45). From these data, we may postulate that there may be a selective advantage for viruses capable of quickly entering the cell. We anticipate that viruses expressing an intermediate density of *env* spikes would have an advantage over multiple rounds of selection due to their ability to quickly achieve a fully bound trimer.

We examined the binding of the virus over short times to determine the bond configuration as a function of gp120 density. Based on the hypothesis that all three gp120 monomers on an *env* spike must be bound to CD4 to eventually lead to viral fusion (5), we measured the likelihood that once a bond is formed, one of the gp120 trimers will become fully bound to CD4, over short times. By multiplying the probability of binding with the probability of forming fully engaged timers, we calculated a surrogate for infective efficiency. We found that for viruses binding to cells with between ~6500 CD4/cell and ~24,000 CD4/cell, a range equivalent to CD4 densities on macrophages in HIV infected patients (46), viruses expressing between 10 and 23 *env* trimers were most efficient in binding with a fully engaged trimer over short times.

This estimate is in close agreement to recent cryo-electron microscopy measurements of 14 ± 7 *env* spikes expressed on the viral surface (13). This optimally efficient density can only be measured while the amount of CD4 in the contact zone is limited when compared to gp120. Once we increase either the density of CD4 or the timescale of the simulation, in the absence of any inactivation process, we note that every virus will have all gp120 trimers in the contact zone fully engaged to CD4. Given the small differences in the binding rate constants of viruses with varying *env* densities, we anticipate that *env* expression on primary viral population in an infected host may be heterogeneous.

We have shown that viruses with as few as eight gp120 trimers will bind with similar rate constants to CD4-coated surfaces as viruses with 72 trimers. Given the results from our long timescale simulations that all viruses will have every gp120 trimer in the contact zone fully engaged given enough time, we would anticipate that there would be no difference in infectivity for viruses with different *env* spike density. Work by Kabat et al. showed that laboratory-adapted (LA) viruses

and primary isolate viruses have different dependence on CD4 density for infectivity (47). We anticipate that this can be explained by the differential selection pressures on the viruses from these two sources resulting in different *env* spike density expressed by these different viral populations. Kabat showed that LA viruses infected equally with host cells with different CD4 densities while primary isolates had increased infectivity when CD4 increased (47). Based on our calculations, we would predict that the LA strains of the virus have been selected for a low gp120 density, so that increasing the CD4 density would have little effect on the probability of forming a fully bound trimer. The primary isolates may have had a higher gp120 density, so viruses would be less likely to form fully bound trimers when binding to low CD4 expressing cells, thereby making these viruses less likely to infect. As Kabat showed, repeating the experiment with cells that have a greater CD4 density increases the infectivity, which would mitigate their limitation in forming a fully bound gp120 trimer.

One limitation to our simulations is that we did not consider viruses with >7 *env* spikes in the contact zone or include the steric hindrance of the cellular receptors that might occur at this density. Presumably, the size of gp120 and CD4 both would affect the interfacial configuration of bonding as we increase the number of gp120 molecules available in the contact area. It might be that significant accumulation of CD4 in the contact zone is not possible, or that at high concentrations of gp120 or CD4, achieving binding of every gp120 in the contact area may be difficult. We anticipate that as the bound CD4 density in the contact area increases, steric hindrance between cellular receptors would increase the time to reach steady state. Hlavacek and co-workers have addressed the role of steric hindrance in multivalent binding (48). They found that steric hindrance increases the time to reach bound states and decreases the total number of available sites. Increasing the number of *env* spikes in the contact zone with steric hindrance would cause us to amend our predictions for binding characteristics of viruses with larger gp120 densities. These calculations would always lead to less binding than predicted here, further reinforcing the conclusion that fewer interactions might lead to more efficient interfacial configurations for viral entry.

We have omitted membrane deformation from our calculations. The cell membrane is known to fluctuate as much as 10 nm on short timescales (microseconds) due solely to thermal energy (49). These fluctuations would appear to be rapid on the timescale of binding, thus leading the membrane to appear as a mean-field to the virus. Recently, Sun and Wirtz showed that when a virus is bound at steady state, the membrane can deform sufficiently to envelop the virus (50). This calculation simplified the gp120 molecules as monomers and calculated the binding deterministically. Thus, small deformations on the order of the size of proteins are possible on small timescales, and large deformations, owing to the reciprocal effect of receptor binding on membrane mechanical deformation, are possible on large timescales. To address the effect of these deformations on viral binding, we would have to include a simulation of the dynamic fluctuations of the membrane as stochastic spatial fluctuations, dictated by the bending modulus of the membrane (51). This is clearly a very difficult calculation which will have to be addressed separately in future work.

This work was supported by National Institutes of Health grants No. HL 18208 and No. HL 087353.

REFERENCES

1. Joint United Nations Program on HIV/AIDS (UNAIDS) and World Health Organization (WHO). 2007. AIDS Epidemic Update: December 2007. UNAIDS.
2. Palella, J. F. J., K. M. Delaney, A. C. Moorman, M. O. Loveless, J. Fuhrer, G. A. Satten, D. J. Aschman, and S. D. Holmberg. 1998. Declining morbidity and mortality among patients with advanced human immunodeficiency virus infection. *N. Engl. J. Med.* 338:853–860.
3. Brooks, G. F., J. S. Butel, and S. A. Morse. 2004. Jawetz, Melnick, & Adelberg's Medical Microbiology, 23rd Ed. Lange Medical Series. McGraw Hill & Company, New York.
4. Kwong, P. D., R. Wyatt, J. Robinson, R. W. Sweet, J. Sodroski, and W. A. Hendrickson. 1998. Structure of an HIV gp120 envelope glycoprotein in complex with the CD4 receptor and a neutralizing human antibody. *Nature.* 393:648–659.
5. Gallo, S. A., C. M. Finnegan, M. Viard, Y. Raviv, A. Dimitrov, S. S. Rawat, A. Puri, S. Durell, and R. Blumenthal. 2003. The HIV Env-mediated fusion reaction. *Biochim. Biophys. Acta.* 1614:36–50.
6. Layne, S. P., M. J. Merges, M. Dembo, J. L. Spouge, and P. L. Nara. 1990. HIV requires multiple gp120 molecules for CD4-mediated infection. *Nature.* 346:277–279.
7. Danieli, T., S. L. Pelletier, Y. I. Henis, and J. M. White. 1996. Membrane fusion mediated by the influenza virus hemagglutinin requires the concerted action of at least three hemagglutinin trimers. *J. Cell Biol.* 133:559–569.
8. Yang, X., S. Kurteva, X. Ren, S. Lee, and J. Sodroski. 2005. Stoichiometry of envelope glycoprotein trimers in the entry of human immunodeficiency virus type 1. *J. Virol.* 79:12132–12147.
9. Gelderblom, H. R. 1991. Assembly and morphology of HIV: potential effect of structure on viral function. *AIDS.* 5:617–637.
10. Briggs, J. A., T. Wilk, R. Welker, H. G. Krausslich, and S. D. Fuller. 2003. Structural organization of authentic, mature HIV-1 virions and cores. *EMBO J.* 22:1707–1715.
11. Zhu, P., E. Chertova, J. J. Bess, J. D. Lifson, L. O. Arthur, J. Liu, K. A. Taylor, and K. H. Roux. 2003. Electron tomography analysis of envelope glycoprotein trimers on HIV and simian immunodeficiency virus virions. *Proc. Natl. Acad. Sci. USA.* 100:15812–15817.
12. Chertova, E., J. J. W. Bess, Jr., B. J. Crise, I. R. Sowder, T. M. Schaden, J. M. Hilburn, J. A. Hoxie, R. E. Benveniste, J. D. Lifson, L. E. Henderson, and L. O. Arthur. 2002. Envelope glycoprotein incorporation, not shedding of surface envelope glycoprotein (gp120/SU), is the primary determinant of SU content of purified human immunodeficiency virus type 1 and simian immunodeficiency virus. *J. Virol.* 76:5315–5325.
13. Zhu, P., J. Liu, J. J. Bess, E. Chertova, J. D. Lifson, H. Grise, G. A. Ofek, K. A. Taylor, and K. H. Roux. 2006. Distribution and three-dimensional structure of AIDS virus envelope spikes. *Nature.* 441: 847–852.
14. English, T. J., and D. A. Hammer. 2004. Brownian adhesive dynamics (BRAD) for simulating the receptor-mediated binding of viruses. *Biophys. J.* 86:3359–3372.
15. Bell, G. I. 1978. Models for the specific adhesion of cells to cells. *Science.* 200:618–627.

16. Caputo, K. E., and D. A. Hammer. 2005. Effect of microvillus deformability on leukocyte adhesion explored using adhesive dynamics simulations. *Biophys. J.* 89:187–200.

17. Hammer, D. A., and S. M. Apte. 1992. Simulation of cell rolling and adhesion on surfaces in shear flow: general results and analysis of selectin-mediated neutrophil adhesion. *Biophys. J.* 63:35–57.

18. King, M. R., and D. A. Hammer. 2001. Multiparticle adhesive dynamics: hydrodynamic recruitment of rolling leukocytes. *Proc. Natl. Acad. Sci. USA.* 98:14919–14924.

19. Krasik, E. F., and D. A. Hammer. 2004. A semianalytic model of leukocyte rolling. *Biophys. J.* 87:2919–2930.

20. Dembo, M., D. C. Torney, K. Saxman, and D. Hammer. 1988. The reaction-limited kinetics of membrane-to-surface adhesion and detachment. *Proc. R. Soc. Lond. B. Biol. Sci.* 234:55–83.

21. Barre-Sinoussi, F., J. C. Chermann, F. Rey, M. T. Nugeyre, S. Chamaret, J. Gruest, C. Dauguet, C. Axler-Blin, F. Vezinet-Brun, C. Rouzioux, W. Rozenbaum, and L. Montagnier. 1983. Isolation of a T-lymphotropic retrovirus from a patient at risk for acquired immune deficiency syndrome (AIDS). *Science.* 220:868–871.

22. Zanetti, G., J. A. G. Briggs, K. Grunewald, Q. J. Sattentau, and S. D. Fuller, 2006. Cryo-electron tomographic structure of an immunodeficiency virus envelope complex in situ. *PLoS Pathogens.* 2:790–797.

23. Ermak, D., and J. McCammon. 1978. Brownian dynamics with hydrodynamic interactions. *J. Chem. Phys.* 69:1352–1360.

24. Berg, H. C. 1993. Random Walks in Biology. Princeton University Press, Princeton, NJ.

25. Bell, G. I., M. Dembo, and P. Bongrand. 1984. Cell adhesion. Competition between nonspecific repulsion and specific bonding. *Biophys. J.* 45:1051–1064.

26. King, M. R., and D. A. Hammer. 2001. Multiparticle adhesive dynamics. Interactions between stably rolling cells. *Biophys. J.* 81:799–813.

27. Matsumoto, M., and T. Nishimura. 1998. Mersenne Twister: a 623-dimensionally equidistributed uniform pseudo-random number generator. *ACM Trans. Model. Comput. Simul.* 8:3–30.

28. Rouse, P. 1953. A theory of linear viscoelastic properties of dilute solutions of coiling polymers. *J. Chem. Phys.* 21:1272–1280.

29. Chang, K. C., and D. A. Hammer. 2000. Adhesive dynamics simulations of sialyl-Lewis$_x$/E-selectin-mediated rolling in a cell-free system. *Biophys. J.* 79:1891–1902.

30. Poignard, P., E. O. Saphire, P. W. Parren, and D. R. Burton. 2001. gp120: Biologic aspects of structural features. *Annu. Rev. Immunol.* 19:253–274.

31. Pal, R., B. C. Nair, G. M. Hoke, M. G. Sarngadharan, and M. Edidin. 1991. Lateral diffusion of CD4 on the surface of a human neoplastic T-cell line probed with a fluorescent derivative of the envelope glycoprotein (gp120) of human immunodeficiency virus type 1 (HIV-1). *J. Cell. Physiol.* 147:326–332.

32. Northrup, S. H., S. A. Allison, and J. A. McCammon. 1984. Brownian dynamics simulation of diffusion-influenced bimolecular reactions. *J. Chem. Phys.* 80:1517–1524.

33. English, T. J., and D. A. Hammer. 2005. The effect of cellular receptor diffusion on receptor-mediated viral binding using Brownian adhesive dynamics (BRAD) simulations. *Biophys. J.* 88:1666–1675.

34. Steffens, C. M., and T. J. Hope. 2004. Mobility of the human immunodeficiency virus (HIV) receptor CD4 and coreceptor CCR5 in living cells: implications for HIV fusion and entry events. *J. Virol.* 78:9573–9578.

35. Clare, B., and D. Kepert. 1986. The closest packing of equal circles on a sphere. *Proc. Roy. Soc. Lond. Math. Phys. Sci.* 405:329–344.

36. Doranz, B. J., S. S. Baik, and R. W. Doms. 1999. Use of a gp120 binding assay to dissect the requirements and kinetics of human immunodeficiency virus fusion events. *J. Virol.* 73:10346–10358.

37. Myszka, D. G., R. W. Sweet, P. Hensley, M. Brigham-Burke, P. D. Kwong, W. A. Hendrickson, R. Wyatt, J. Sodroski, and M. L. Doyle. 2000. Energetics of the HIV gp120–CD4 binding reaction. *Proc. Natl. Acad. Sci. USA.* 97:9026–9031.

38. Viard, M., I. Parolini, M. Sargiacomo, K. Fecchi, C. Ramoni, S. Ablan, F. W. Ruscetti, J. M. Wang, and R. Blumenthal. 2002. Role of cholesterol in human immunodeficiency virus type 1 envelope protein-mediated fusion with host cells. *J. Virol.* 76:11584–11595.

39. Popik, W., T. M. Alce, and W. C. Au. 2002. Human immunodeficiency virus type 1 uses lipid raft-colocalized CD4 and chemokine receptors for productive entry into CD4$^+$ T cells. *J. Virol.* 76:4709–4722.

40. Liao, Z., L. M. Cimakasky, R. Hampton, D. H. Nguyen, and J. E. Hildreth. 2001. Lipid rafts and HIV pathogenesis: host membrane cholesterol is required for infection by HIV type 1. *AIDS Res. Hum. Retroviruses.* 17:1009–1019.

41. Platt, E. J., J. P. Durnin, and D. Kabat. 2005. Kinetic factors control efficiencies of cell entry, efficacies of entry inhibitors, and mechanisms of adaptation of human immunodeficiency virus. *J. Virol.* 79:4347–4356.

42. Haim, H., I. Steiner, and A. Panet. 2007. Time frames for neutralization during the human immunodeficiency virus type 1 entry phase, as monitored in synchronously infected cell cultures. *J. Virol.* 81:3525–3534.

43. Dragic, T., V. Litwin, G. P. Allaway, S. R. Martin, Y. Huang, K. A. Nagashima, C. Cayanan, P. J. Maddon, R. A. Koup, J. P. Moore, and W. A. Paxton. 1996. HIV-1 entry into CD4$^+$ cells is mediated by the chemokine receptor CC–CKR-5. *Nature.* 381:667–673.

44. Samson, M., F. Libert, B. J. Doranz, J. Rucker, C. Liesnard, C.-M. Farber, S. Saragosti, C. Lapoumeroulie, J. Cognaux, C. Forceille, G. Muyldermans, C. Verhofstede, G. Burtonboy, M. Georges, T. Imai, S. Rana, Y. Yi, R. J. Smyth, R. G. Collman, R. W. Doms, G. Vassart, and M. Parmentier. 1996. Resistance to HIV-1 infection in Caucasian individuals bearing mutant alleles of the CCR-5 chemokine receptor gene. *Nature.* 382:722–725.

45. Ugolini, S., I. Mondor, P. W. Parren, D. R. Burton, S. A. Tilley, P. J. Klasse, and Q. J. Sattentau. 1997. Inhibition of virus attachment to CD4$^+$ target cells is a major mechanism of T cell line-adapted HIV-1 neutralization. *J. Exp. Med.* 186:1287–1298.

46. Nokta, M. A., X. D. Li, J. Nichols, M. Mallen, A. Pou, D. Asmuth, and R. B. Pollard. 2001. Chemokine/CD4 receptor density ratios correlate with HIV replication in lymph node and peripheral blood of HIV-infected individuals. *AIDS.* 15:161–169.

47. Kabat, D., S. L. Kozak, K. Wehrly, and B. Chesebro. 1994. Differences in CD4 dependence for infectivity of laboratory-adapted and primary patient isolates of human immunodeficiency virus type 1. *J. Virol.* 68:2570–2577.

48. Hlavacek, W. S., R. G. Posner, and A. S. Perelson. 1999. Steric effects on multivalent ligand-receptor binding: exclusion of ligand sites by bound cell surface receptors. *Biophys. J.* 76:3031–3043.

49. Brown, F. L. H. 2003. Regulation of protein mobility via thermal membrane undulations. *Biophys. J.* 84:842–853.

50. Sun, S. X., and D. Wirtz. 2006. Mechanics of enveloped virus entry into host cells. *Biophys. J.* 90:L10–L12.

51. Helfrich, W. 1990. Elasticity and thermal undulations of fluid films of amphiphiles. *In* Liquids and Interfaces, Les Houches XLVIII, 1988. J. Charvolin, J. F. Joanny, and J. Zinn-Justin, editors. Elsevier Science Publishers, Dordrecht, The Netherlands.